2015

Effect of Residual Stresses on the Stress Intensity Factors for Cracks Near Fillet Welds

Changyuan Du
Lehigh University

Effect of Residual Stresses on the Stress Intensity Factors for Cracks Near Fillet Welds

By

Changyuan Du

A Thesis

Presented to the Graduate and Research Committee

Of Lehigh University

In Candidacy for the Degree of

Master of Science

In

Mechanical Engineering

Lehigh University

May 2016

This thesis is accepted and approved in partial fulfillment of the requirements for the Master of Science.

_____

Date

_____

Thesis Advisor

_____

Chairperson of Department

Acknowledgments

I wish to express my thanks to my advisor Prof. Herman F. Nied, for his support on my thesis. And also thank the Prof. Saribay, for his help on my research.

Also, thank my parents for their support.

Table of Contents

List of Figures

List of Tables

Abstract

In this study, Stress Intensity Factors are calculated for cracks located at the toe of a fillet weld subjected to residual stresses due to the welding. The welding model used in this study is based on Longitudinal stiffener test specimens. The meshes generated for these models were obtained from the commercial code HYPERMESH. The welding heat transfer simulation and calculation of the welding residual stresses used the explicit FE commercial code SYSWELD. The residual stresses obtained from the welding simulations for the uncracked configuration were applied as an initial pressure on the crack surface in the subsequent fracture mechanics analyses with cracks. The calculation of Stress Intensity Factors in the cracked configuration utilize a specialized finite element program, FRAC2D, which was developed at Lehigh University. For the results in this study, two different meshes and two different materials are considered and the value of the Stress Intensity Factors, for different crack lengths are calculated during the fracture mechanics analyses.

Chapter 1. Introduction

1.1 Background

Researchers have long known that welding residual stresses play a significant role in the fatigue behavior in engineering structures [1-4]. Berge [1] calculated the residual stresses in a welded joint, Baumgartner [2] calculated residual stresses in Longitudinal Stiffener models. Williams [3] considered the stress state for angular corners in plates, and Bussu [4] consider the effect of residual stress on crack growth for Friction stir welding.

For fracture mechanics, Stress Intensity Factors represent a single parameter that can be used for making accurate predictions concerning subcritical crack growth and unstable fracture. The accurate prediction of crack growth behavior is an important consideration when assessing the reliability of welded structures. Thus, researchers have developed analytical [5-7] and numerical [8-9] models to calculate Stress Intensity Factors for weld structures with cracks. Stefanescu, et.al, [5], analyzed fatigue for cracks at holes [5], while Pommier [6] analyzed a semi-elliptical crack in a semi-infinite body and Nguyen, et.al, [7] analyzed residual stress of fatigue life. Besides analytical fracture models, Dexter, et.al, [8] analyzed a two-dimensional numerical model of welded stiffened panels to predict the effect of residual stress on the Stress Intensity Factors. Krishnakumar [9] analyzed crack propagation in a three-dimensional of aluminium alloy plates. However, the residual stress considered above is rather hypothetical and not predicted by precise numerical simulation. So the above models could not realistically predict the real welding residual stresses and take into account the real residual stress field into the SIF calculations.

In this study, the focus is to use the residual stresses due to fusion welding for direct computation of the Stress Intensity Factors for cracks adjacent to a fillet weld. Finite element analyses that properly takes into account the severe stress gradient at a crack tip, provides a powerful tool for fracture mechanics calculations. In this study, simulation of the welding process is first performed and the resulting residual stresses are introduced into the fracture mechanics analysis for calculating the Stress Intensity Factors in the cracked model. In creating the finite element models, the geometry and the mesh used in the welding and fracture models were generated using the commercial code HYPERMESH [10]. Welding simulation, used to calculate the welding residual stresses, were obtained from the explicit FE commercial code SYSWELD [11]. The calculation of Stress intensity factors for the cracked configuration utilized a specialized finite element program FRAC2D, which was developed at Lehigh University. The advantage of using a code like FRAC2D, which contains the correct stress singularity at the crack tip, is that specialized crack tip meshes do not need to be created. Thus, automatic mesh generation can be used, without regard to the crack tip stress singularity. The computed results from the SYSWELD analyses include: (1) the temperature distributions during the welding process; (2) temperature distribution after the welding process, i.e., during cooling; (3) Von Mises stress distribution during welding; (4) Von Mises stress distribution during cooling; (5) residual stress $\boldsymbol{\sigma_{xx}}$ distribution during welding process; (6) residual stress $\boldsymbol{\sigma_{xx}}$ distribution during cooling process; (7) residual stress $\boldsymbol{\sigma_{xx}}$ along the line of the crack after cooling. Finally, FRAC2D was used to directly calculate the Stress intensity factors for different crack lengths using the residual stresses obtained from the SYSWELD results.

1.2 Longitudinal Stiffeners Model

In this study, the focus is on the thermo-mechanical and fracture behavior of an example Longitudinal stiffener which contains general features for analyzing weld fracture behavior. Figure 1.1 shows the Longitudinal stiffener test specimen with top and bottom stiffeners welded to the flat plate in three welding passes [15]. The black bold line in Figure 1.2 shows that crack initiates at the toe of the welds and grows vertically through the flat plate. Thus, the simulations in this study will focus on the cracking behavior in the neighborhood of the weld toe.

Figure 1.1 Longitudinal Stiffener test specimen [15]

A complete finite element model of the detailed 3-D welding process for this test specimen, with multiple weld passes, would require a large mesh resulting in considerable computational resources [16]. Thus, the simpler 2-D model shown in Figure 1.2 was used in this study. It was felt that this much simpler 2-D model could reasonably represent the detailed welding behavior and resulting residual stresses in the neighborhood of the weld toe. The models include an 8.5 mm thick, 30 mm long vertical bar, a 6 mm thick, 60 mm long horizontal plate, and a triangular fillet weld with an 8.5 mm base and 8.5 mm in height. In addition, the model also contained a small 0.25 mm gap between the horizontal plate and vertical bar. The gap can be filled with filler metal, or left as an air gap during the

analysis. For this study, the gap is modeled with the same material properties as the filler metal.

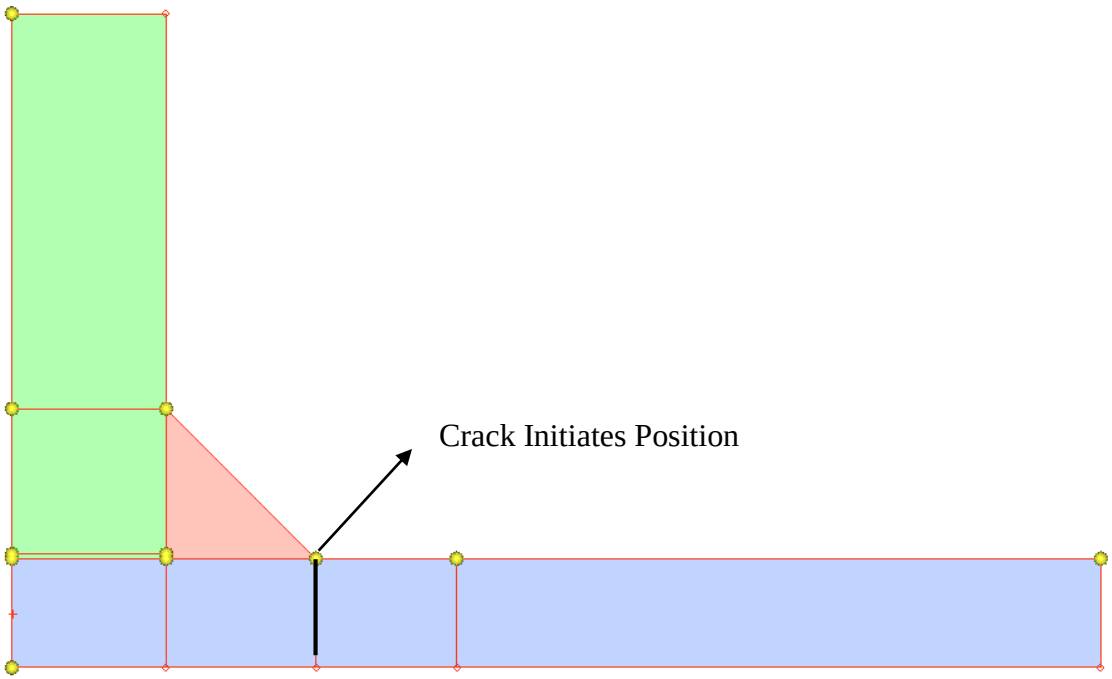

Figure 1.2 The geometry of the model

Chapter 2. Numerical Analysis

In this study, the geometry and the mesh used for the finite element models were developed using HYPERMESH [10]. The finite element entities of the models are transferred to SYSWELD using a Template called DATA_ASC_SET from *.HM HYPERMESH file *.ASC SYSWELD file to file *.ASC SYSWELD file. The transferred file contains the topology of the model. The finite element entities for the models are also transferred to ANSYS, by way of transformed ASCII files, using the *.HM file from HYPERMESH and *.CDB ANSYS file. The transferred file contains the topology of the models. After simulation of the welding process in SYSWELD, the residual stresses are exported from SYSWELD as a *.LIS file and imported as an initial pressure into the ANSYS/FRAC2D. The methodology in this study uses the same topology of the models for welding simulation and fracture mechanics analysis. Thus, it ensures good integration between the two simulations.

2.1 Mesh Analysis

HYPERMESH is a more expedient tool to create complex geometry and mesh and export models to other different environment, compared to SYSWELD. Thus, HYPERMESH is used to the generate meshes for the 2D finite element meshes used in this study. For the entire finite element model, the ‘Quad4’ element type and the ‘Tria3’ element type of element was generated in HYPERMESH.

Crack initiation often occurs in the neighborhood of the weld fillet, in the Heat Affected Zone (HAZ), close to the toe of the weld [15], so dense meshes need to be used in the area close to the toe of the weld, while coarser meshes can be used for the rest of the welded structure. In this study, two different meshes were used to test how well the mesh quality and density influenced the value of the welding residual stresses. The first mesh is shown in Figure 2.3. This mesh uses a uniform mesh refinement that contains 2109 nodes and 732 elements; the second mesh used in this study is a finer mesh with 4290 nodes and 1464 elements.

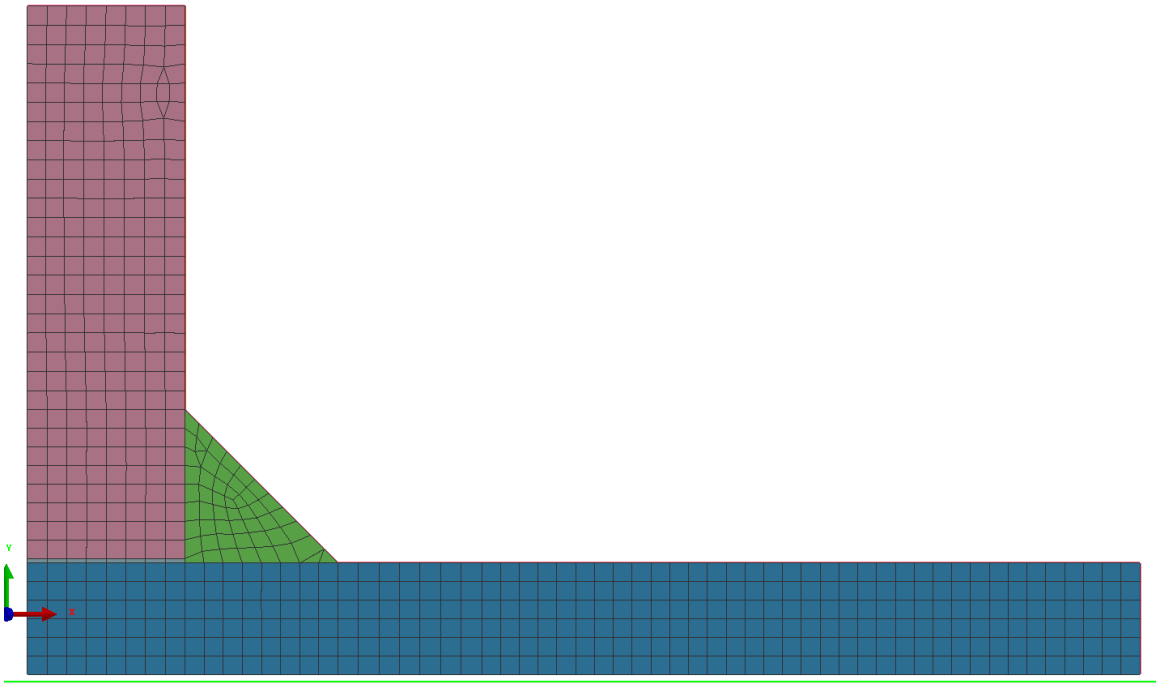

Figure 2.1 Uniform Mesh

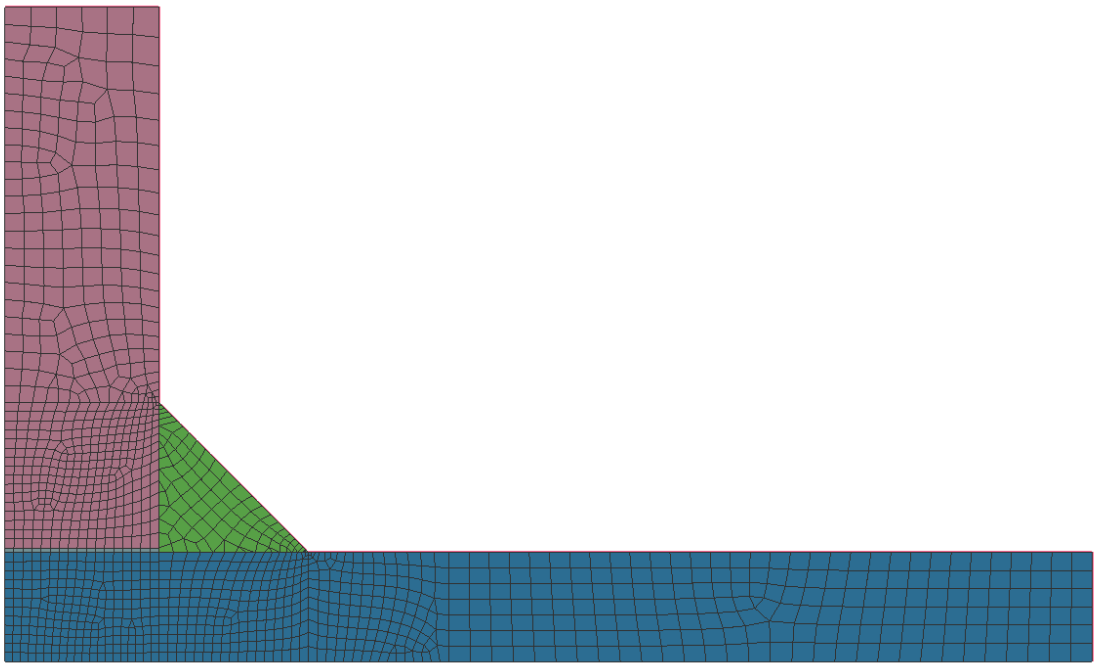

Figure 2.2 Finer mesh

2.2 Welding Analysis

SYSWELD was used to simulate the welding process in two steps**.** The first step of the welding simulation is the heat transfer analysis. After the first step, the results from the temperature distribution are stored and used for the subsequent stress simulation. The second step is the mechanical analysis (stresses), where the temperature distribution from the previous heat transfer calculations are used as input. After the temperature distribution during welding has been determined, the residual stresses can be calculated by performing a nonlinear thermal stress analysis of the structure.

Welding simulation for the determination of residual stresses using the commercially available finite element codes requires specifying a moving heat source [15], and its path of motion. SYSWELD helps to automate the process of building the moving

heat source, input of the material properties, and specifying the mechanical boundary conditions [12]. All of this greatly simplifies creating the welding simulation models. The residual stresses are insensitive to the welding process parameters, especially the temperature gradients as the liquid melt cools and solidifies. In SYSWELD, the heat source can be modeled using 2-D, Axisymmetric, or 3-D models [15]. It has been shown [14], that 2-D models of moving heat sources provide excellent simulation for Pèclet Numbers greater than 10 ($Pe = vl/\kappa$), where $v =$ heat source velocity, l is a characteristic length, plate thickness, and κ is the thermal diffusivity given by $\kappa = \lambda/(\rho C_p)$, where λ is the thermal conductivity, ρ the density and C_p the heat capacity.

Single weld pass weld models were used in this study to simplify the welding process simulations. The Welding Parameters that were used include: the welding speed of 6.329mm/s, the weld pool width of 12mm and welding penetration of 6 mm. The welding Energy/Unit length was specified to be 1632.0 J/mm. the time of duration for welding is 3.16s, with the initial temperature assumed to be ambient temperature, i.e., 20 ℃. Convection and radiation boundary conditions were maintained on all surfaces during heating and cooling.

2.3 Fracture Mechanics Analysis

FRAC2D are used to compute the stress intensity factors for specified crack lengths after the welding simulation, while ANSYS [13] is being used to simply reformat the files for use in FRAC2D. In this analysis, the finite element nodes, elements and material properties, as usually required for an ANSYS stress analysis, are exported from HYPERMESH in the appropriate ANSYS format. The residual stresses obtained from the

welding simulation were imported to ANSYS as an initial pressure acting on the crack surface. The black bold line in Figure 2.5 shows that crack initiates at the toe of the welds and grows vertically through the flat plate. There are no other loads on the model. After the initial stress is applied as pressure to the crack surfaces, the finite element program ANSYS to FRAC2D converter was used to compute the correct consistent nodal forces that are equivalent to the pressure distribution to yield the correct Stress Intensity Factors.

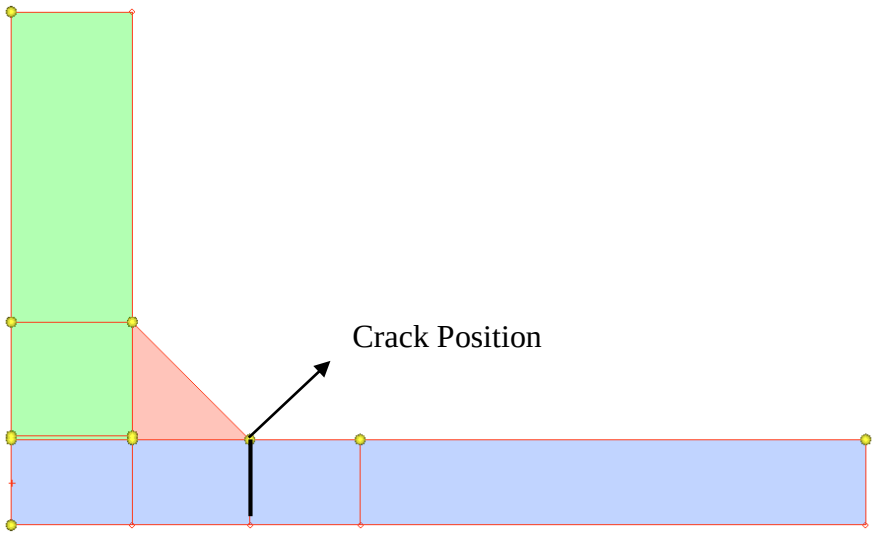

Figure 2.3 the crack position in the model

In this study, the models used in welding simulation and mechanical analysis has a difference: the SYSWELD model is uncracked while the FRAC2D model is cracked. So additional nodes need to be added in the FRAC2D model to create a crack which will properly open up with the pressure values from the SYSWELD model. For example, uncracked configuration is shown in Figure 2.6(a) and cracked configuration is shown in Figure 2.6(b). The node 1 is the crack tip node and the vertical bold black line shown in Figure 2.6(b) is the crack. Nodes 2, 3, 4 are duplicated into Nodes 2, 3, 4, 5, 6, 7 and Nodes1, 2, 3, 4 and Nodes 1, 5, 6, 7 constitute two crack surface in HYPERMESH

manually. And the residual stress component σ_{xx} calculated from welding simulation is used as the initial pressure in fracture analysis.

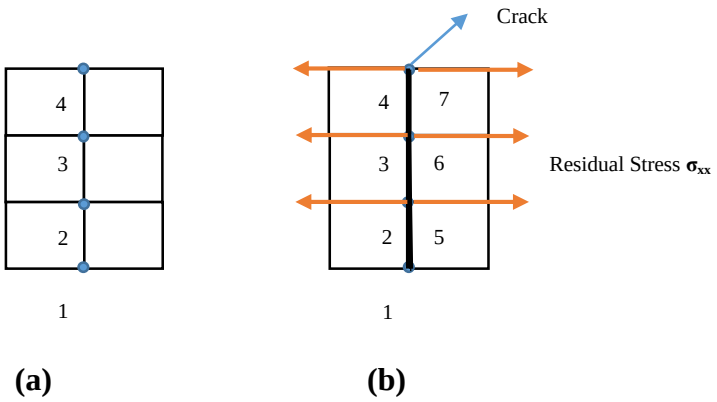

Figure 2.4 (a) uncracked meshes configuration (b) cracked meshes configuration

In this study, HYPERMESH uses the 'Quad4' element type and the 'Tria3' element type to generate model. Figure 2.5 shows the detail of the 'Quad4' element type [10]. Figure 2.6 shows the detail of the 'Tria3' element type [10]. SYSWELD uses the quadratic elements. Figure 2.7 shows the detail of the quadratic elements. ANSYS [13] uses quadratic elements 'Plane82' shown in Figure 2.8. While, FRAC2D uses cubic elements shown in Figure 2.9.

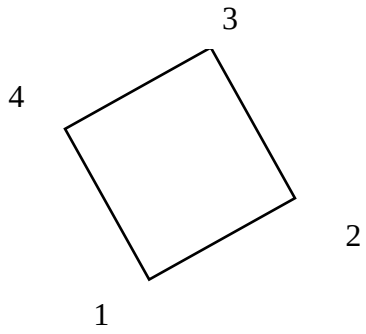

Figure 2.5 Quad4, quadratic 2D elements with 4 nodes ordered in HYPERMESH [10]

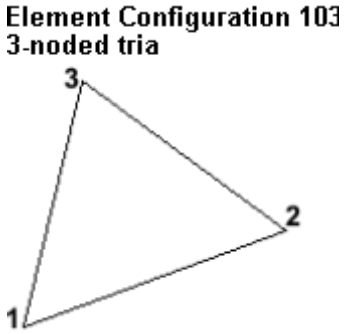

Figure 2.6 Tria3, 2D triangular elements with 3 nodes ordered in HYPERMESH [10]

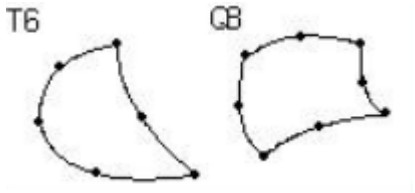

Figure 2.7 the quadratic elements in SYSWELD

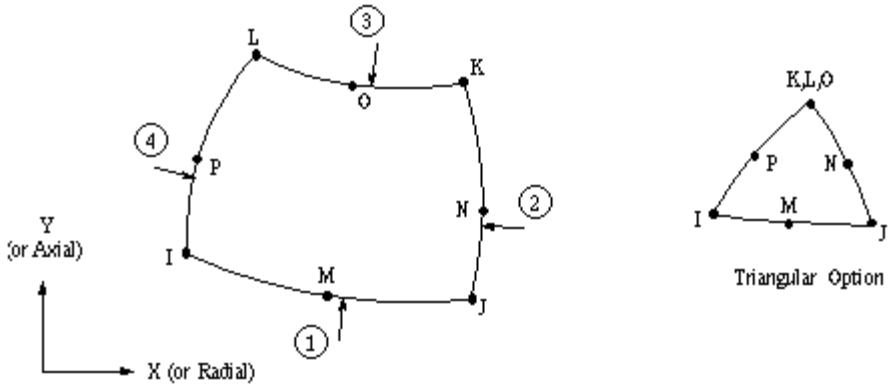

Figure 2.8 Plane82 2-d element type in ANSYS [13]

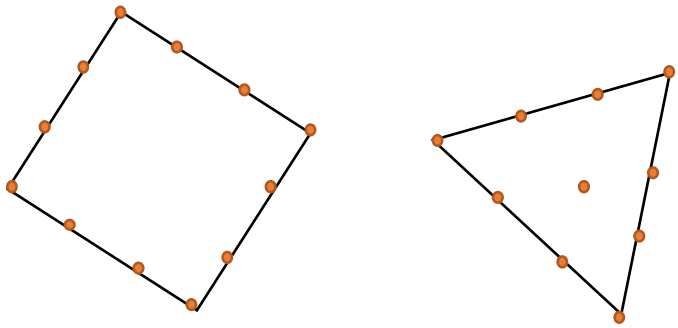

Figure 2.9 Cubic element type in FRAC2D

Thus, in order to calculate the stress intensity factors in FRAC2D, the finite element information needs to be transferred from ANSYS to FRAC2D. The ANSYS to FRAC2D converter puts additional nodes at the correct coordinates for the elements used in FRAC2D. The converter program also converts Pressure Loading, Prescribed Displacements, Concentrated forces, and Temperature loading for the new FRAC2D mesh. In this study, 3 pressure values calculated from 3-nodes quadratic element in ANSYS are converted to 4 pressure values (consistent node forces) in FRAC2D.

Chapter 3. Parameters of the Model

The basic parameters used in this study: model material property information, clamping conditions are presented below.

3.1 Model material

In this study, the welded structure and the weld deposition material are the same material. For structural carbon steel S355J2G3 metallurgical phase changes occur, resulting in transformation plasticity. This is in contrast to 316L austenitic stainless steel, which does not exhibit metallurgical phase transformations that result in additional volumetric strains. The thermal property of these two alloys are available in the SYSWELD database. Table 3.1 shows the mechanical properties of these two alloys on room temperature.

Table 3.1 Mechanical property of S355J2G3 and 316L

	Yield Strength(MPa)	Tensile Strength(MPa)	Elongation(%)
S355J2G3	355	630	22
316L	170	485	35

3.2 Clamping Condition

The mechanical boundary condition strongly influence the value of the residual stress. In this study, the model is constrained as shown in Figure 3.1. Note that all nodes on the bottom of the bar are fixed in a direction along the y axis (U_y=0) and all nodes on the vertical line are fixed in a direction along the x axis (U_x=0).

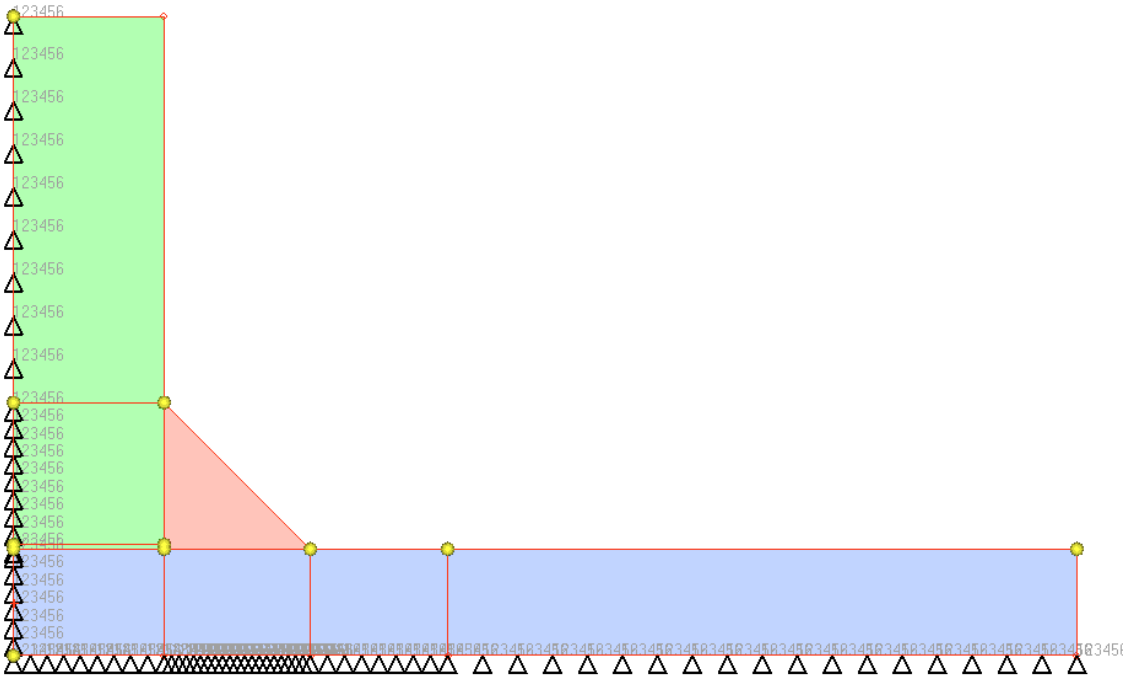

Figure 3.1 Clamping Conditions of the model

Chapter 4. Simulation Results and Conclusion

The results from the welding simulations and fracture mechanics analyses for two different meshes is presented in this chapter. The computed results include: (1) the temperature distributions during the welding process; (2) temperature distribution after the welding process, i.e., during cooling; (3) Von Mises stress distribution during welding; (4) Von Mises stress distribution during cooling ; (5) residual stress $\boldsymbol{\sigma_{xx}}$ distribution during welding process; (6) residual stress $\boldsymbol{\sigma_{xx}}$ distribution during cooling process; (7) residual stress $\boldsymbol{\sigma_{xx}}$ along the line of the crack after cooling; (8) Stress intensity factors for different crack lengths.

4.1 Uniform mesh for S355J2G3

Figure 4.1 shows the transient temperature distributions that occurs during the welding process as the heat source approaches the cross-section plane. Figure 4.2 shows the transient temperature distribution after weld arc has passed the cross-section of interest. Figure 4.3 shows the von Mises stress distribution during welding process, while Figure 4.4 shows the von Mises stress distribution during cooling and in particular at 3600s after the structure has completely cooled. Figure 4.5 shows the residual stress $\boldsymbol{\sigma_{xx}}$ distribution during the welding process. Figure 4.6 shows the residual stress $\boldsymbol{\sigma_{xx}}$ distribution as cooling occurs, and in particular after 3600s. Figure 4.7 shows residual stress $\boldsymbol{\sigma_{xx}}$ along the crack after cooling. In Figure 4.6(3), there is a stress concentration near the welding toe at t=3600 s, but the residual stress $\boldsymbol{\sigma_{xx}}$ on the welded toe is in compression which may not be correct.

To check the validity of the negative residual stress $\boldsymbol{\sigma_{xx}}$ around the welded toe, residual stresses $\boldsymbol{\sigma_{xx}}$, $\boldsymbol{\sigma_{xy}}$, $\boldsymbol{\sigma_{yy}}$ from the upper surface measured from welded toe in x direction are calculated in Figure 4.8. On the top surface which is free surface, $\boldsymbol{\sigma_{xy}}$, $\boldsymbol{\sigma_{yy}}$ should be zero, but the result shown in Figure 4.8, $\boldsymbol{\sigma_{xy}}$, $\boldsymbol{\sigma_{yy}}$ are zero after x=10.5. So the negative value of the residual stress $\boldsymbol{\sigma_{xx}}$ is incorrect. The reason is that the boundary condition near the welded toe with changed geometry may be failure. In this study, the crack is still set on the welded toe initially. The future work will consider where the crack initiation most likely to occur. Figure 4.9 shows Stress intensity factors (Mpa/$\sqrt{M}$) of different crack length measured from welded toe. Negative value occurs in the Figure 4.9. In this study, the model does not include crack surface contact.

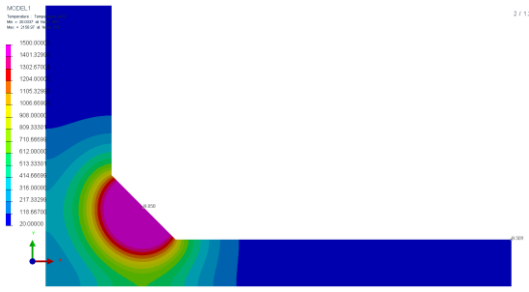

(1)

(2)

(3)

Figure 4.1 Temperature distribution during welding with the Uniform mesh for S355J2G3 (1) at t=1.26s (2) at t=2.52s (3) at t=3.16s

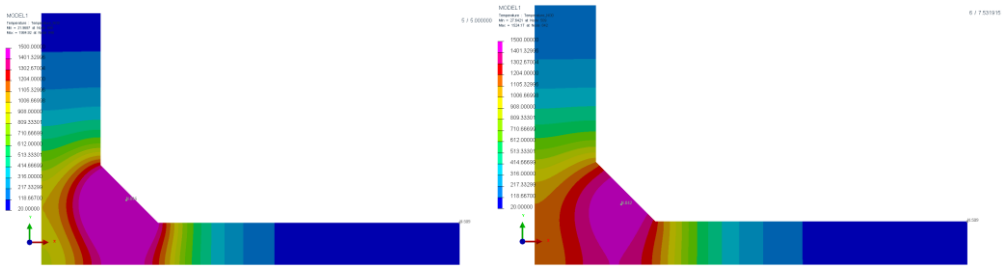

(1) (2)

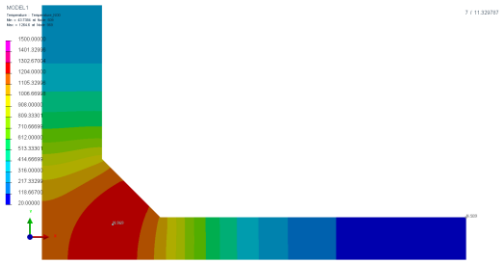

(3)

Figure 4.2 Temperature distribution during cooling with the Uniform mesh for S355J2G3 (1) at t=5 s (2) at t=7 s (3) at t=10s

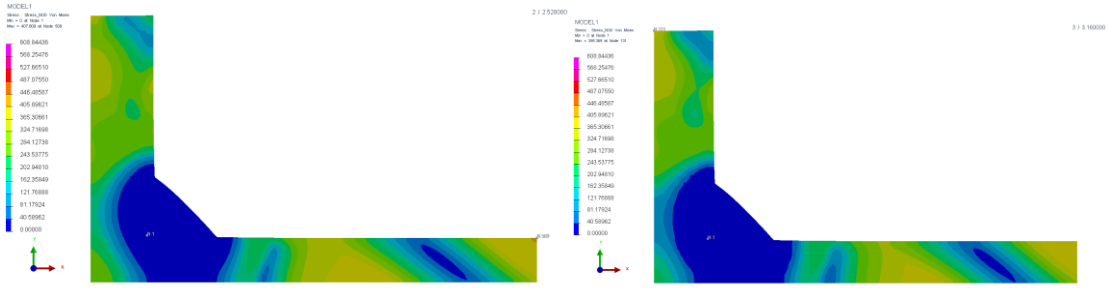

(1) (2)

Figure 4.3 von Mises stress distribution during welding with the Uniform mesh for S355J2G3 (1) at t=2.52s (2) at t=3.16s

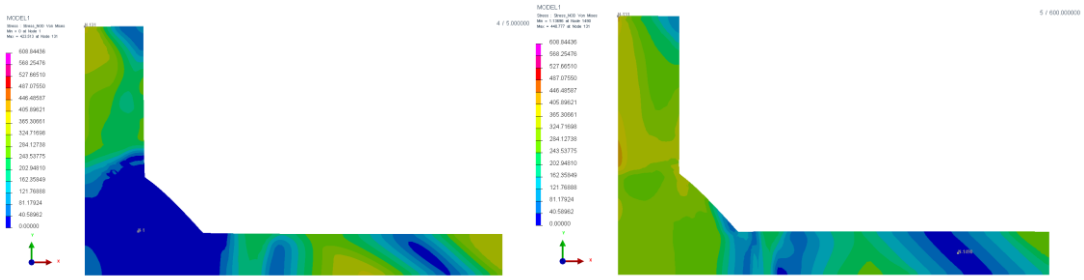

(1) (2)

(3)

Figure 4.4 von Mises stress distribution during cooling process with the Uniform mesh for S355J2G3 (1) at t=5 s (2) at t=600 s (3) at t= 3600 s

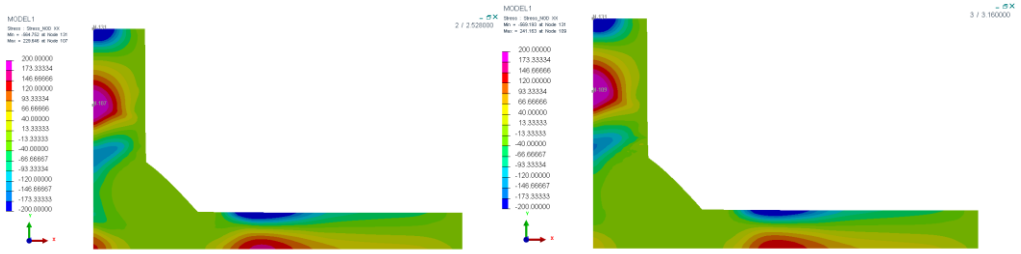

(1) (2)

Figure 4.5 residual stress σ_{xx} distribution during welding with the Uniform mesh for S355J2G3 (1) at= 2.52 (2) at t=3.16

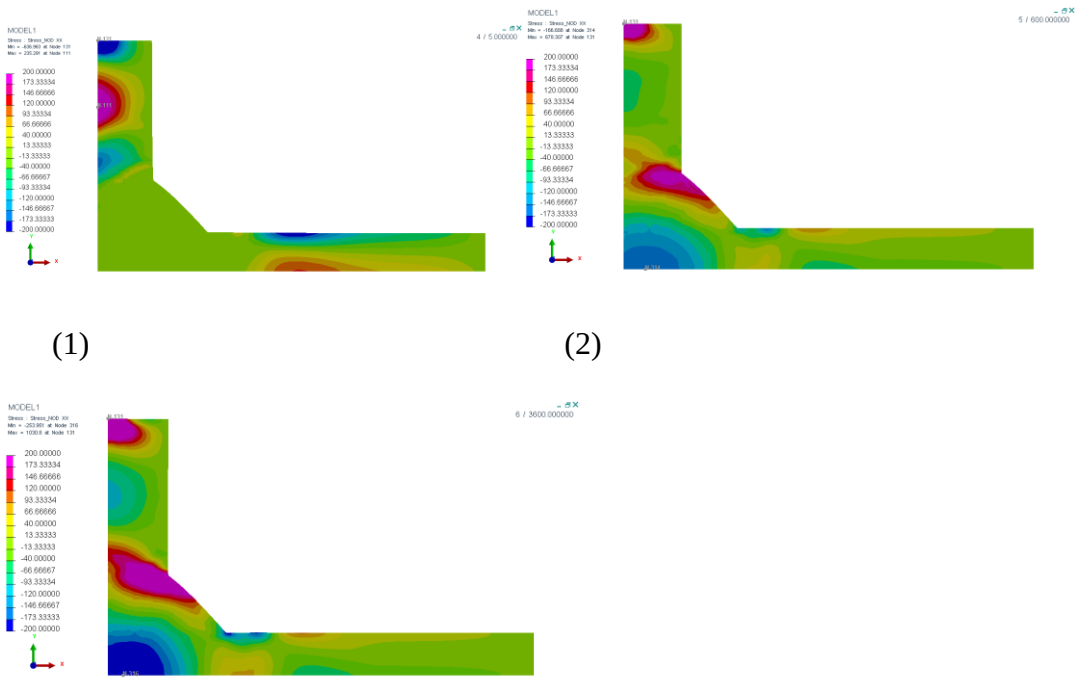

(1) (2)

(3)

Figure 4.6 residual stress σ_{xx} distribution during cooling with the Uniform mesh for S355J2G3 (1) at t=5s (2) at t=600 s (3) at t=3600s

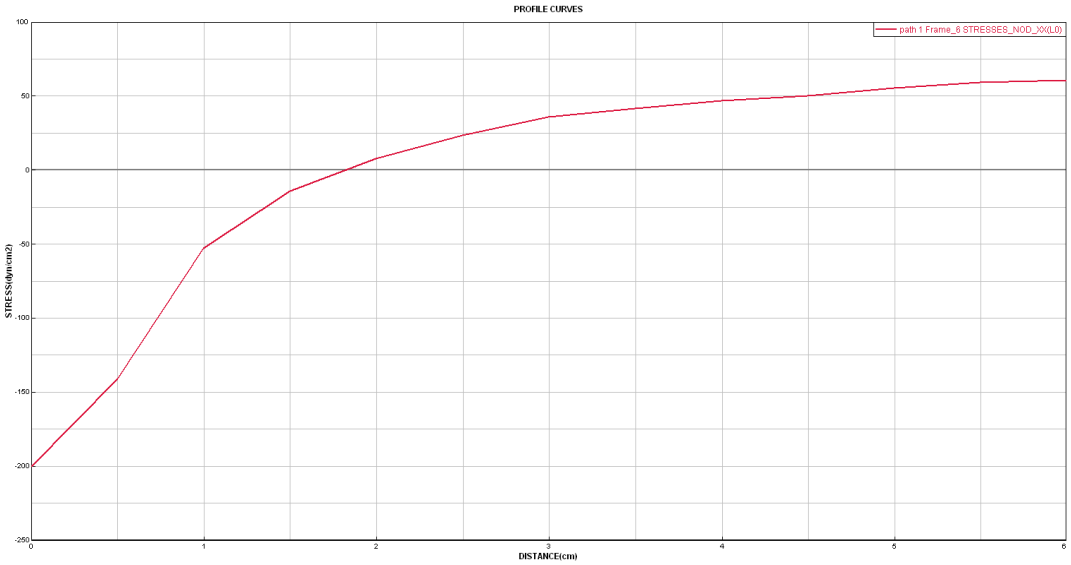

Figure 4.7 residual stress σ_{xx} measured from welded toe in y direction after cooling of uniform mesh with S355J2G3

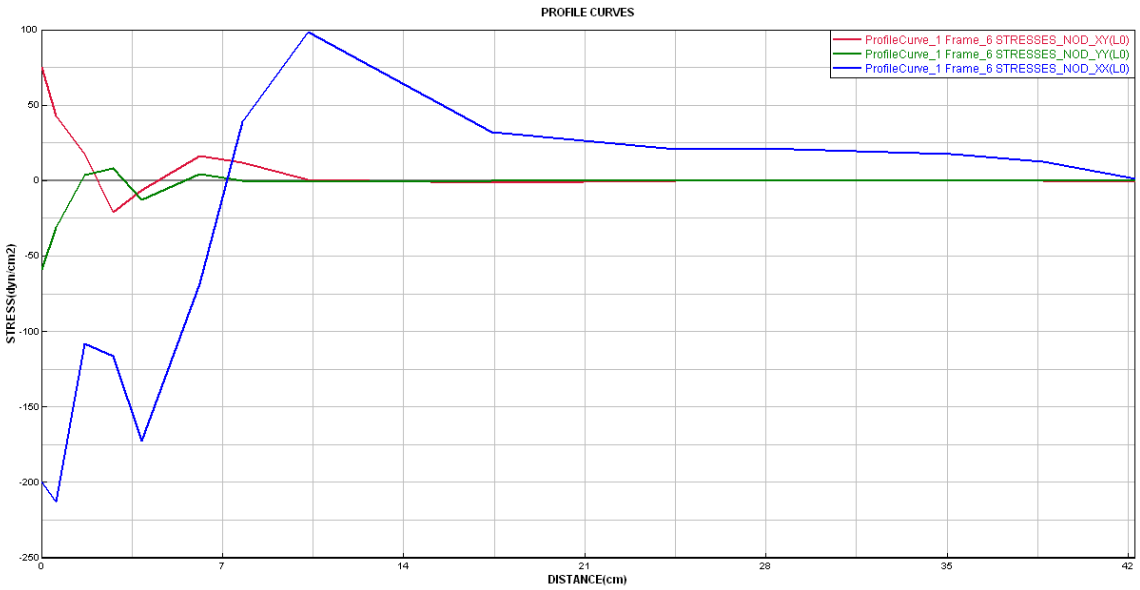

Figure 4.8 residual stresses σ_{xx}, σ_{xy}, σ_{yy} from the upper surface measured from welded toe in x direction

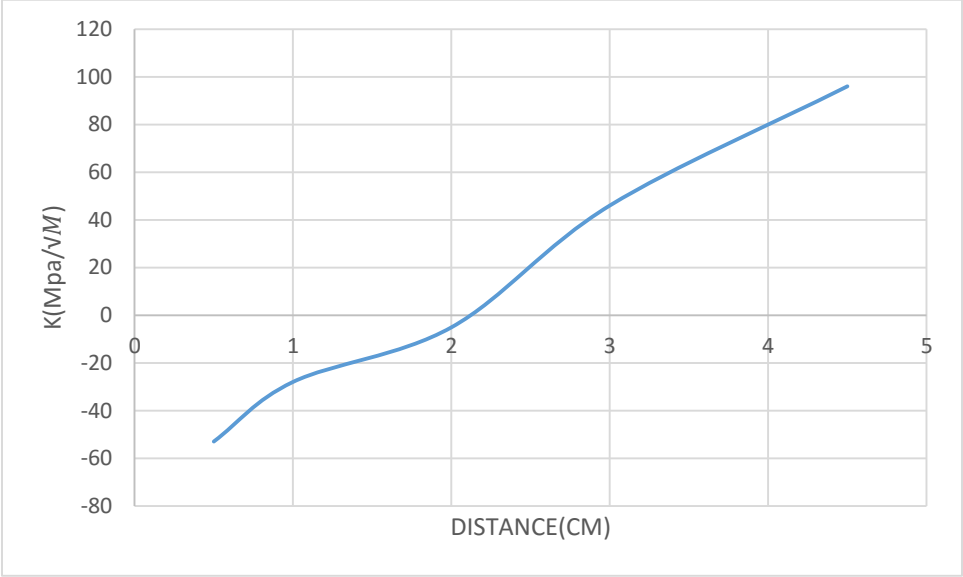

Figure 4.9 Stress intensity factors K (Mpa/$\sqrt{M}$) of different crack length measured from welded toe in Y direction

4.2 Uniform mesh with 316L

Figure 4.10 shows the transient temperature distributions that occurs during the welding process as the heat source approaches the cross-section plane. Figure 4.11 shows the transient temperature distribution after weld arc has passed the cross-section of interest. Figure 4.12 shows the von Mises stress distribution during welding process, while Figure 4.13 shows the von Mises stress distribution during cooling and in particular at 3600s after the structure has completely cooled. Figure 4.14 shows the residual stress $\boldsymbol{\sigma_{xx}}$ distribution during the welding process. Figure 4.15 shows the residual stress $\boldsymbol{\sigma_{xx}}$ distribution as cooling occurs, and in particular after 3600s. Figure 4.16 shows residual stress $\boldsymbol{\sigma_{xx}}$ along the crack after cooling. In Figure 4.15(3), there is a stress concentration near the welding toe at t=3600 s, but the residual stress $\boldsymbol{\sigma_{xx}}$ on the welded toe is in compression which may not be correct. To check the validity of the negative residual stress $\boldsymbol{\sigma_{xx}}$ around the welded toe, residual stresses $\boldsymbol{\sigma_{xx}}$, $\boldsymbol{\sigma_{xy}}$, $\boldsymbol{\sigma_{yy}}$ from the upper surface measured from welded toe in x direction are calculated in Figure 4.17. The Figure 4.17 shows that $\boldsymbol{\sigma_{xy}}$, $\boldsymbol{\sigma_{yy}}$ are not zero before x=7. So the negative value of the residual stress $\boldsymbol{\sigma_{xx}}$ is incorrect. Figure 4.18 shows Stress intensity factors (Mpa/$\sqrt{M}$) of different crack length measured from welded toe.

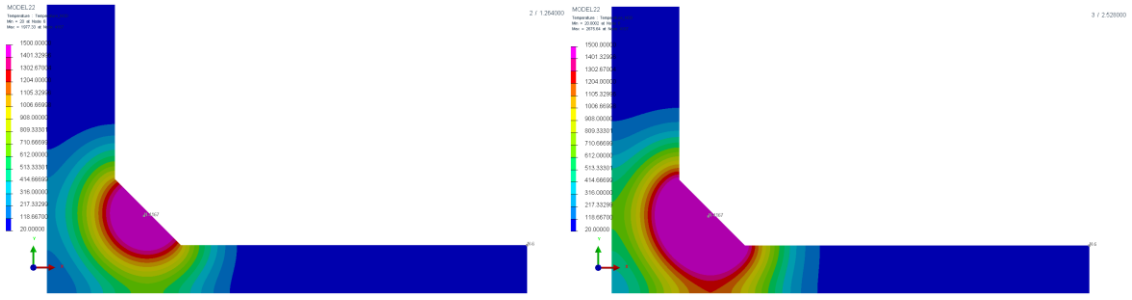

(1) (2)

(3)

Figure 4.10 Temperature distribution during welding with the Uniform mesh for 316L (1) at t=1.26s (2) at t=2.52s (3) at t=3.16s

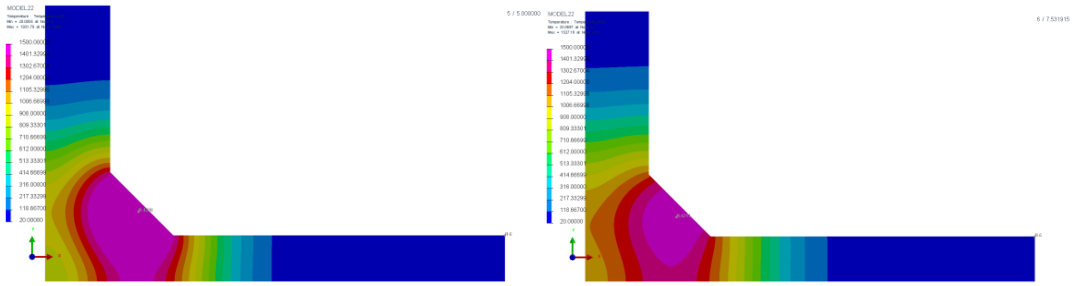

(1) (2)

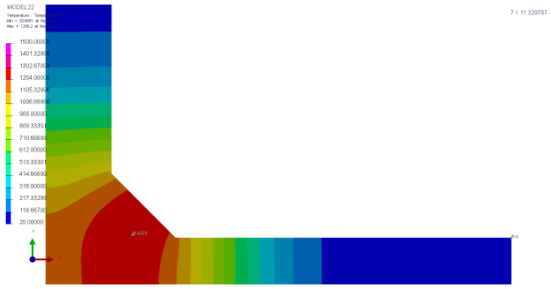

(3)

Figure 4.11 Temperature distribution during cooling with the Uniform mesh for 316L (1) at t=5 s (2) at t=7 s (3) at t=10s

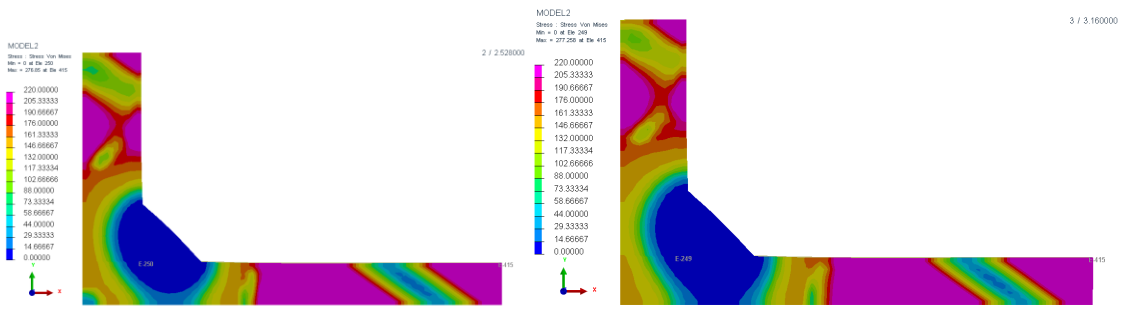

(1) (2)

Figure 4.12 von Mises stress distribution during welding with the Uniform mesh for 316L (1) at t=2.52s (2) at t=3.16s

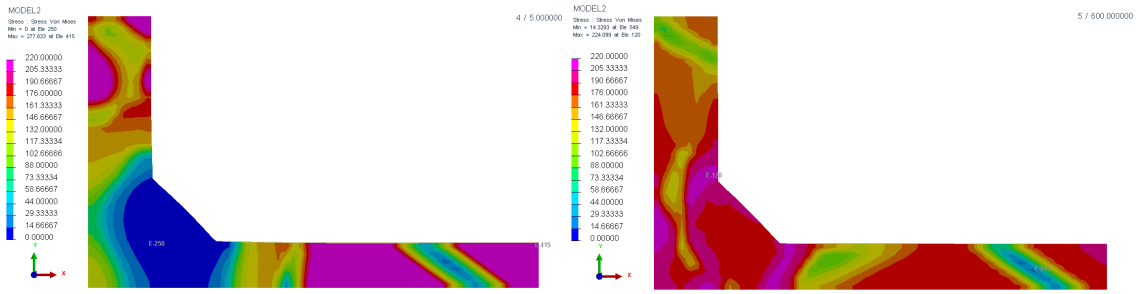

(1) (2)

(3)

Figure 4.13 von Mises stress distribution during cooling with the Uniform mesh for 316L (1) at t=5 s (2) at t=600 s (3) at t= 3600 s

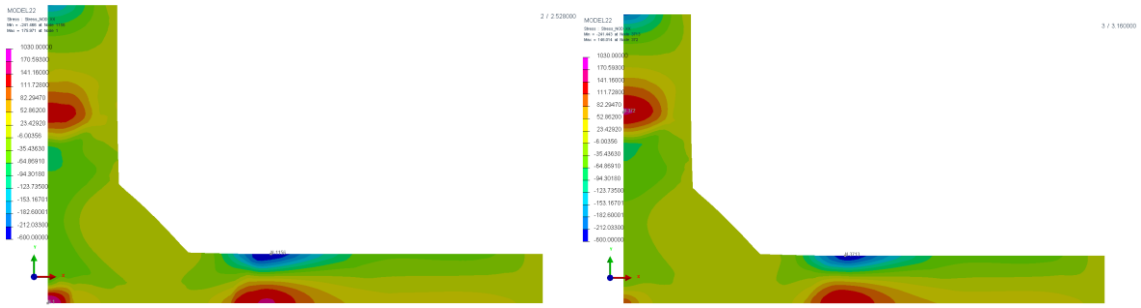

(1) (2)

Figure 4.14 residual stress σ_{xx} distribution during welding with the Uniform mesh for 316L (1) at= 2.52 (2) at t=3.16

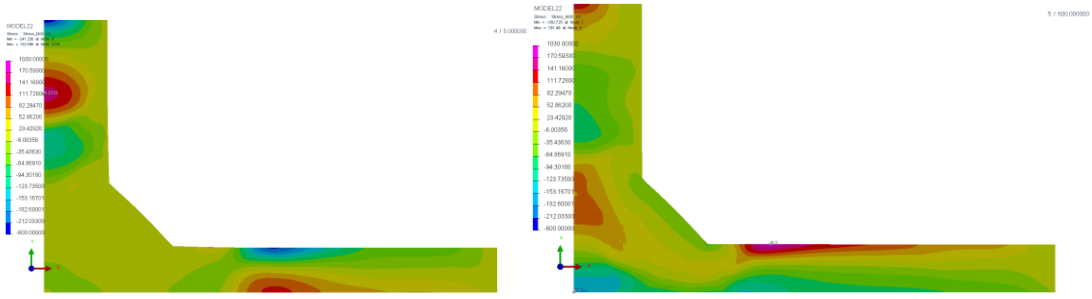

(1) (2)

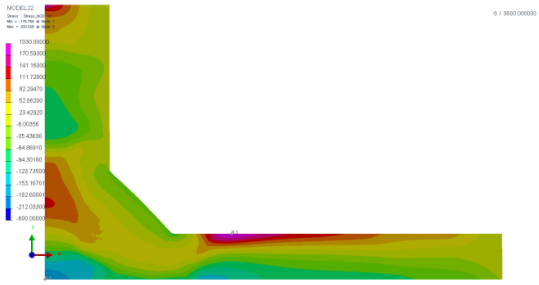

(3)

Figure 4.15 residual stress σ_{xx} distribution during cooling process with the Uniform mesh for 316L (1) at t=5s (2) at t=600 s (3) at t=3600s

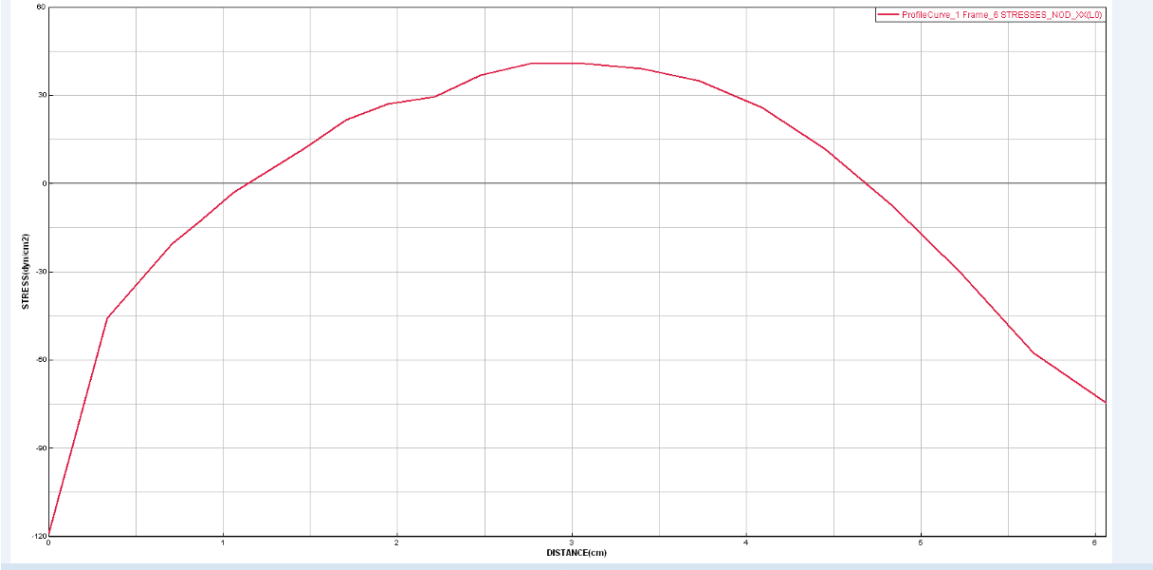

Figure 4.16 residual stress σ_{xx} measured from welded toe in y direction after cooling

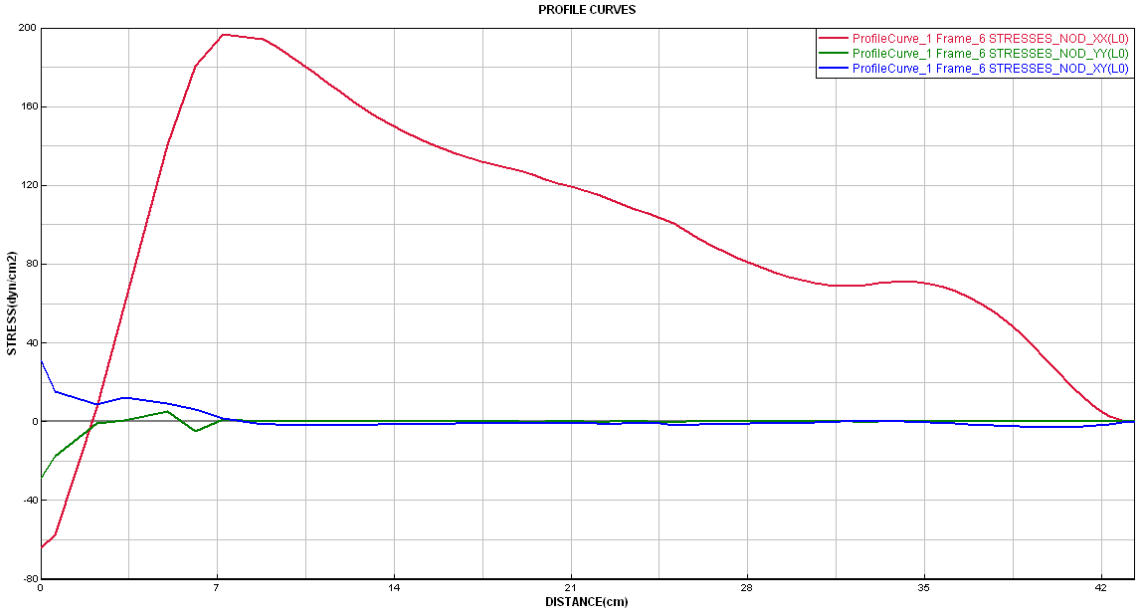

Figure 4.17 residual stresses σ_{xx}, σ_{xy}, σ_{yy} from the upper surface measured from welded toe in x direction

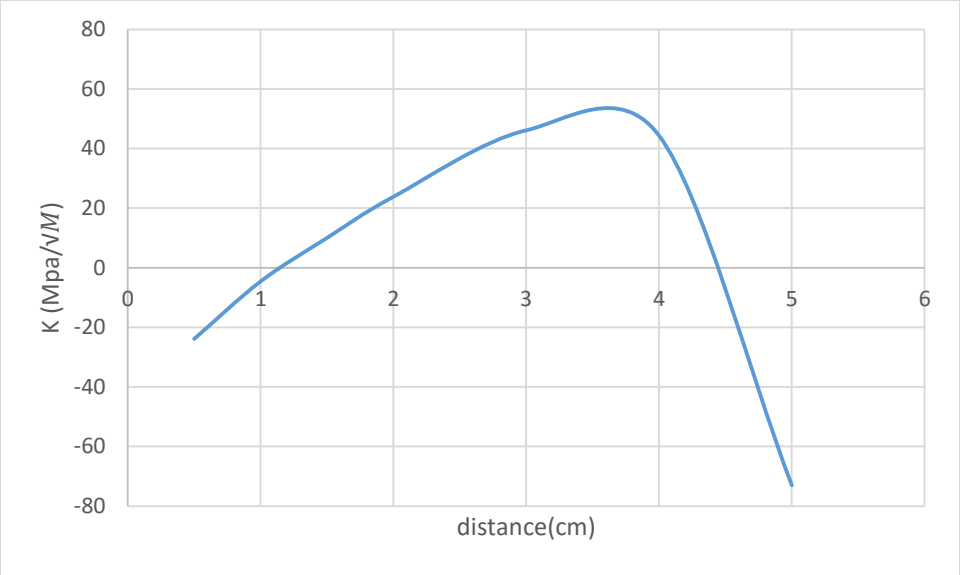

Figure 4.18 Stress intensity factors K (Mpa/$\sqrt{M}$) of different crack length measured from welded toe in Y direction

4.3 Finer mesh with S355J2G3

Figure 4.19 shows the transient temperature distributions that occurs during the welding process as the heat source approaches the cross-section plane. Figure 4.20 shows the transient temperature distribution after weld arc has passed the cross-section of interest. Figure 4.21 shows the von Mises stress distribution during welding process, while Figure 4.22 shows the von Mises stress distribution during cooling and in particular at 3600s after the structure has completely cooled. Figure 4.23 shows the residual stress $\boldsymbol{\sigma_{xx}}$ distribution during the welding process. Figure 4.24 shows the residual stress $\boldsymbol{\sigma_{xx}}$ distribution as cooling occurs, and in particular after 3600s. Figure 4.25 shows residual stress $\boldsymbol{\sigma_{xx}}$ along the crack after cooling. In Figure 4.24(3), there is a stress concentration near the welding toe at t=3600 s, but the residual stress $\boldsymbol{\sigma_{xx}}$ on the welded toe is in compression which may not be correct. To check the validity of the negative residual stress $\boldsymbol{\sigma_{xx}}$ around the welded toe,

residual stresses $\boldsymbol{\sigma_{xx}}$, $\boldsymbol{\sigma_{xy}}$, $\boldsymbol{\sigma_{yy}}$ from the upper surface measured from welded toe in x direction are calculated in Figure 4.26. The Figure 4.26 shows that $\boldsymbol{\sigma_{xy}}$, $\boldsymbol{\sigma_{yy}}$ are not zero before x=10.5. So the negative value of the residual stress $\boldsymbol{\sigma_{xx}}$ is incorrect. Figure 4.27 shows Stress intensity factors (Mpa/$\sqrt{M}$) of different crack length measured from welded toe.

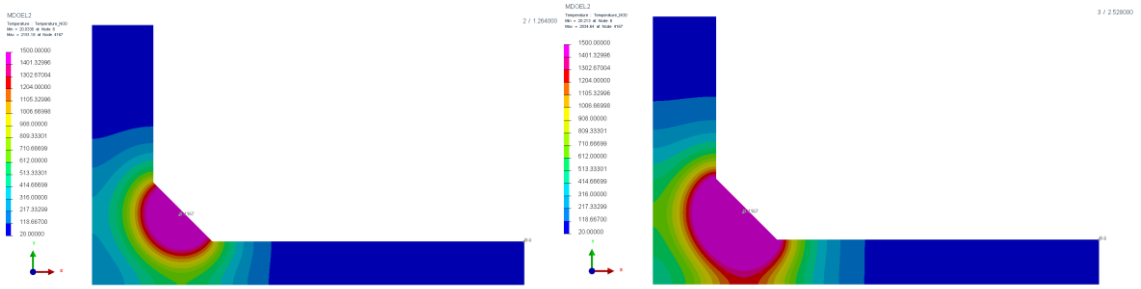

(1) (2)

(3)

Figure 4.19 Temperature distribution during welding with the finer mesh for S355J263 (1) at t=1.26s (2) at t=2.52s (3) at t=3.16s

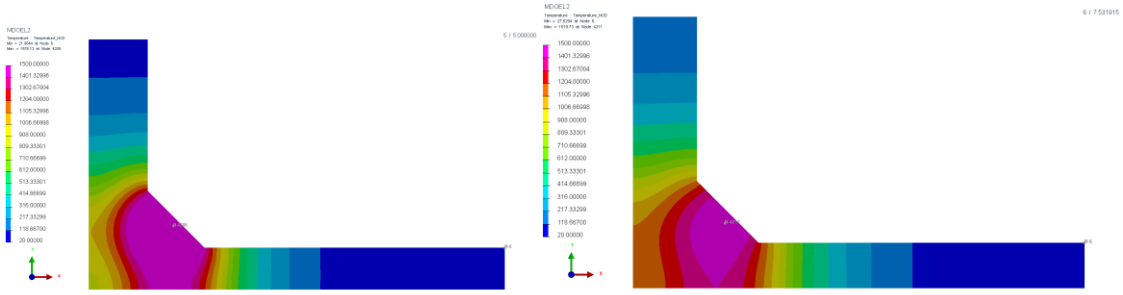

(1) (2)

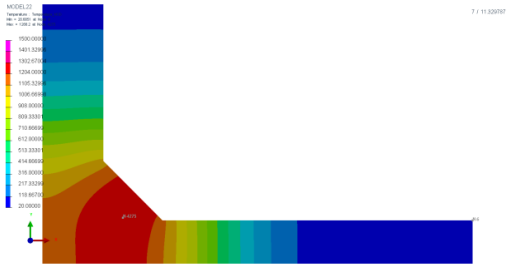

(3)

Figure 4.20 Temperature distribution during cooling process with the finer mesh for S355J263 (1) at t=5 s (2) at t=7 s (3) at t=10s

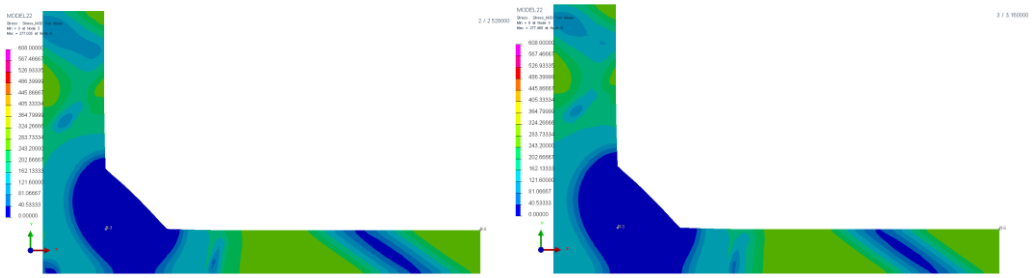

(1) (2)

Figure 4.21 von Mises stress distribution during welding process with the finer mesh for S355J263 (1) at t=2.52s (2) at t=3.16s

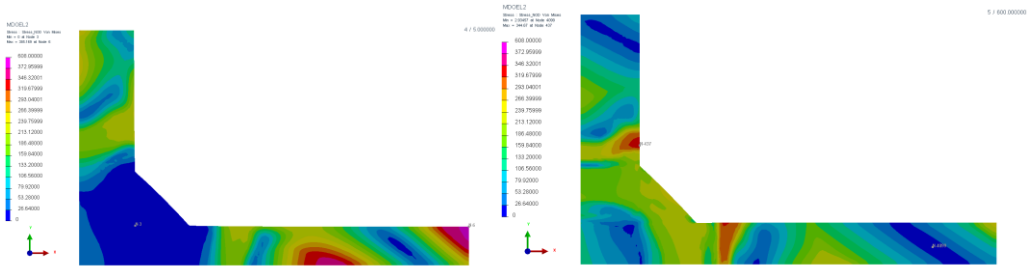

(1) (2)

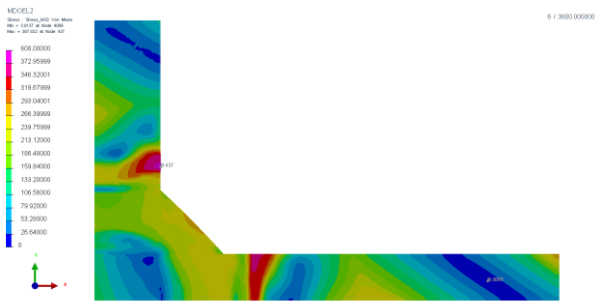

(3)

Figure 4.22 von Mises stress distribution during cooling with the finer mesh for S355J263 (1) at t=5 s (2) at t=600 s (3) at t= 3600 s

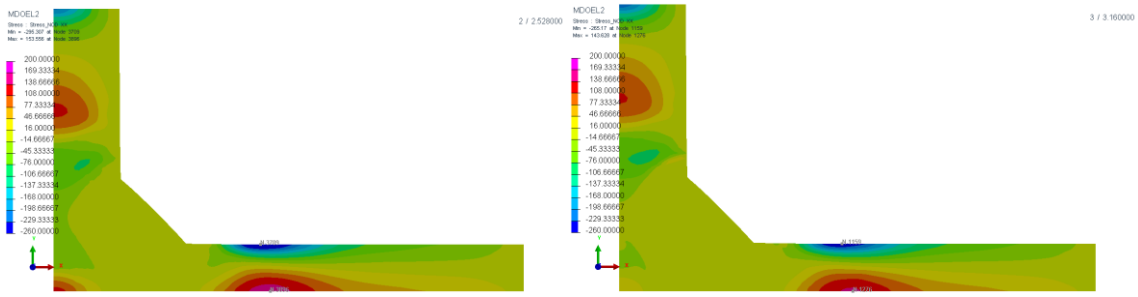

(1) (2)

Figure 4.23 residual stress σ_{xx} distribution during welding with the finer mesh for S355J263 (1) at= 2.52 (2) at t=3.16

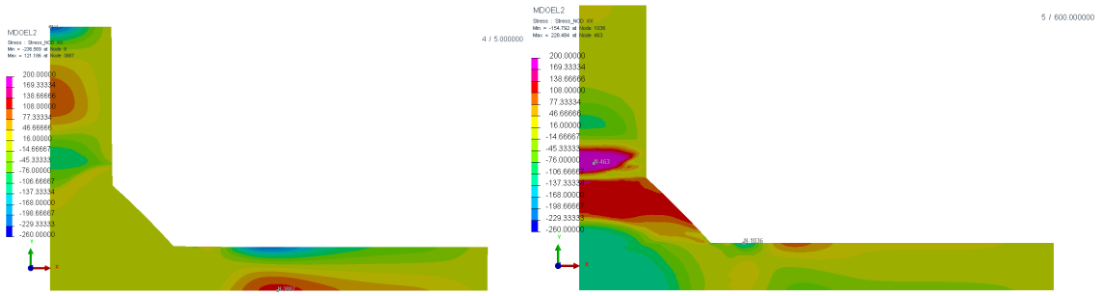

(1) (2)

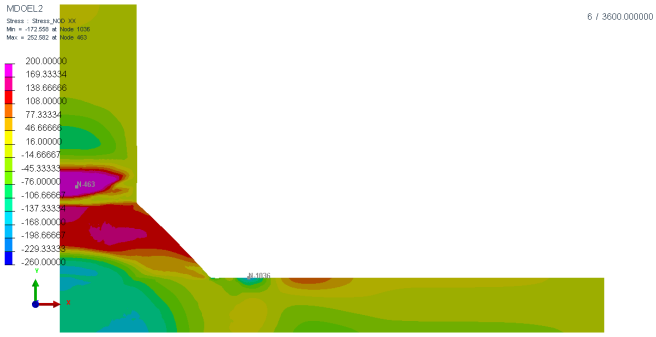

(3)

Figure 4.24 residual stress σ_{xx} distribution during cooling with the finer mesh for S355J263 (1) at t=5s (2) at t=600 s (3) at t=3600s

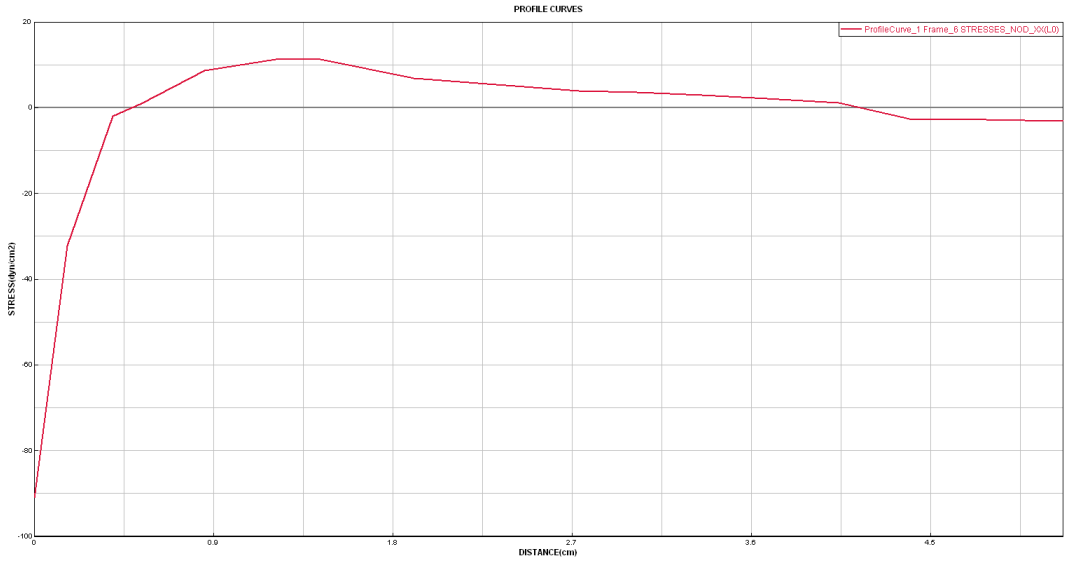

Figure 4.25 residual stress σ_{xx} measured from welded toe in y direction after cooling

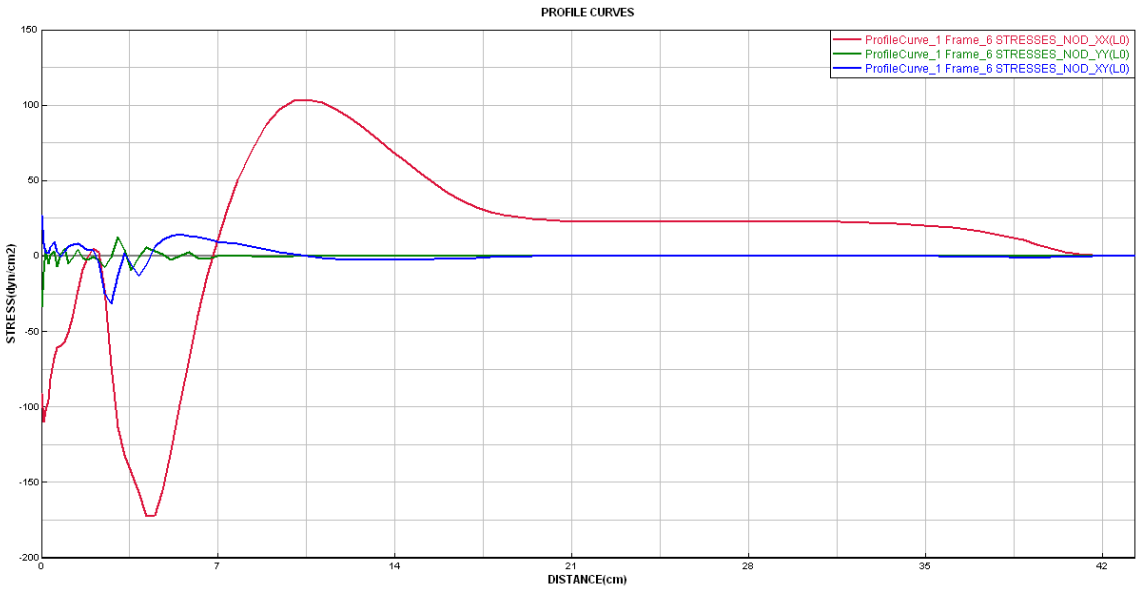

Figure 4.26 residual stresses σ_{xx}, σ_{xy}, σ_{yy} from the upper surface measured from welded toe in x direction

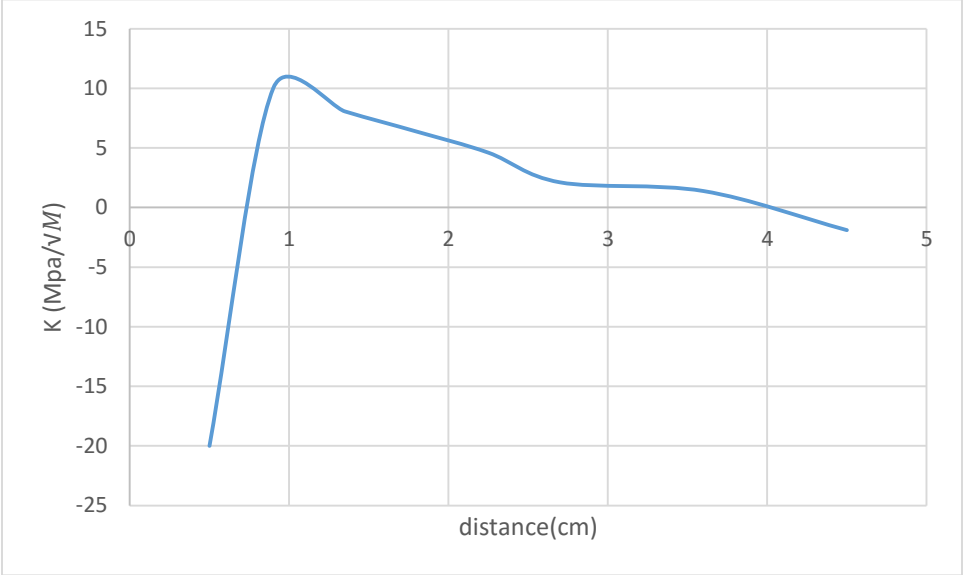

Figure 4.27 Stress intensity factors K (Mpa/$\sqrt{M}$) of different crack length measured from welded toe in Y direction

4.4 Finer mesh with 316L

Figure 4.28 shows the transient temperature distributions that occurs during the welding process as the heat source approaches the cross-section plane. Figure 4.29 shows the transient temperature distribution after weld arc has passed the cross-section of interest. Figure 4.30 shows the von Mises stress distribution during welding process, while Figure 4.31 shows the von Mises stress distribution during cooling and in particular at 3600s after the structure has completely cooled. Figure 4.32 shows the residual stress $\boldsymbol{\sigma_{xx}}$ distribution during the welding process. Figure 4.33 shows the residual stress $\boldsymbol{\sigma_{xx}}$ distribution as cooling occurs, and in particular after 3600s. Figure 4.34 shows residual stress $\boldsymbol{\sigma_{xx}}$ along the crack after cooling. In Figure 4.33(3), there is a stress concentration near the welding toe at t=3600 s, but the residual stress $\boldsymbol{\sigma_{xx}}$ on the welded toe is in compression which may not be correct. To check the validity of the negative residual stress $\boldsymbol{\sigma_{xx}}$ around the welded toe, residual stresses $\boldsymbol{\sigma_{xx}}$, $\boldsymbol{\sigma_{xy}}$, $\boldsymbol{\sigma_{yy}}$ from the upper surface measured from welded toe in x direction are calculated in Figure 4.35. The Figure 4.35 shows that $\boldsymbol{\sigma_{xy}}$, $\boldsymbol{\sigma_{yy}}$ are not zero before x=7. So the negative value of the residual stress $\boldsymbol{\sigma_{xx}}$ is incorrect. Figure 4.36 shows Stress intensity factors (Mpa/$\sqrt{M}$) of different crack length measured from welded toe.

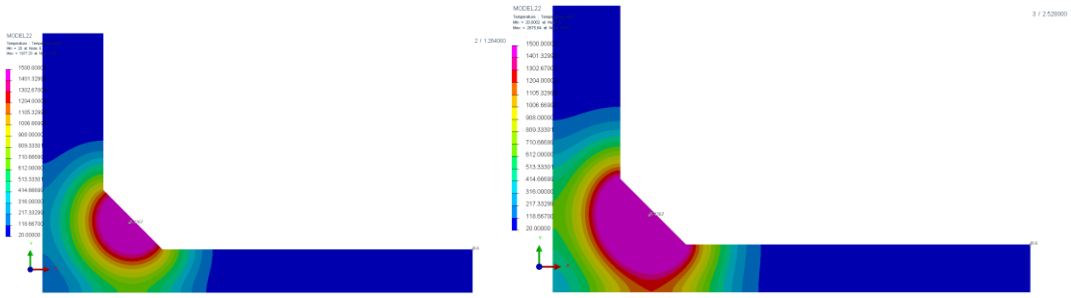

(1) (2)

(3)

Figure 4.28 Temperature distribution during welding with the finer mesh for 316L (1) at t=1.26s (2) at t=2.52s (3) at t=3.16s

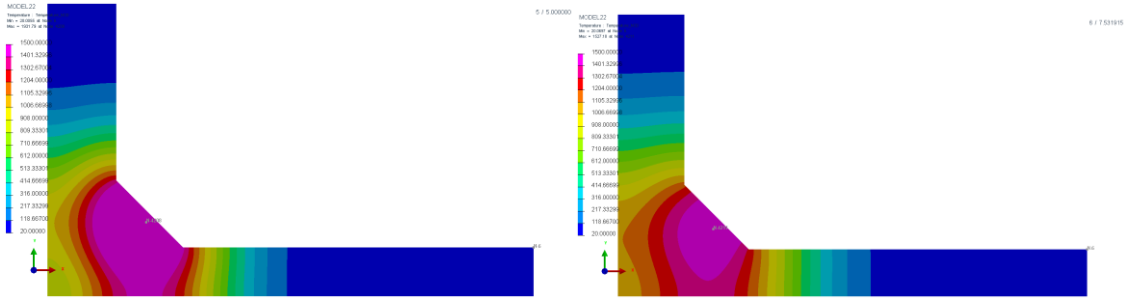

(1) (2)

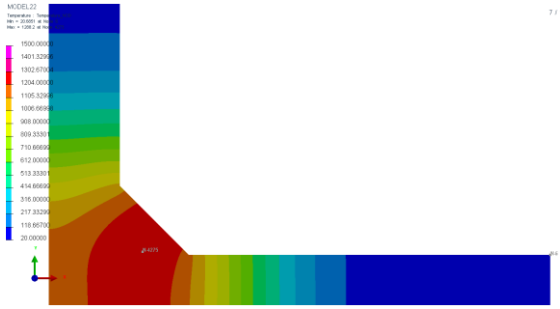

(3)

Figure 4.29 Temperature distribution during cooling with the finer mesh for 316L (1) at t=5 s (2) at t=7 s (3) at t=10s

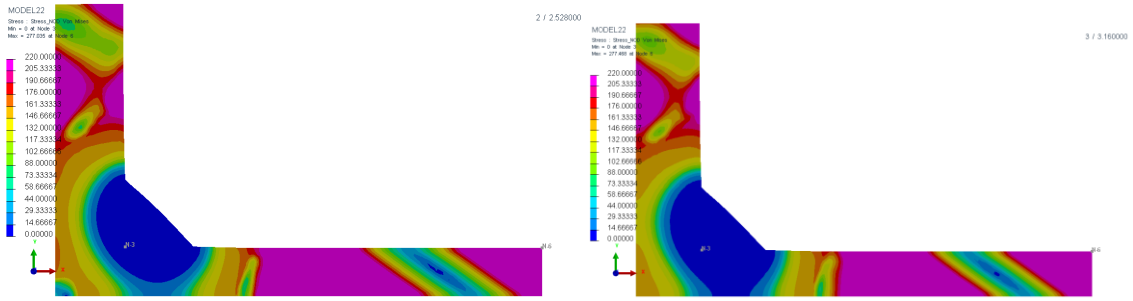

(1) (2)

Figure 4.30 von Mises stress distribution during welding with the finer mesh for 316L (1) at t=2.52s (2) at t=3.16s

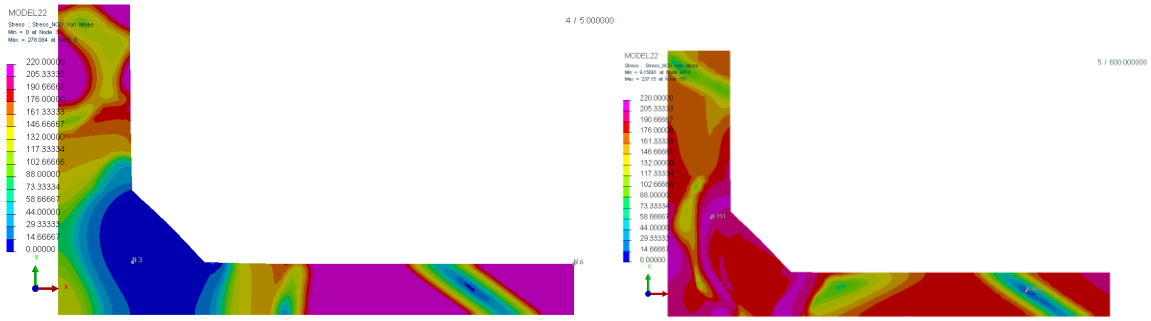

(1) (2)

(3)

Figure 4.31 von Mises stress distribution during cooling with the finer mesh for 316L (1) at t=5 s (2) at t=600 s (3) at t= 3600 s

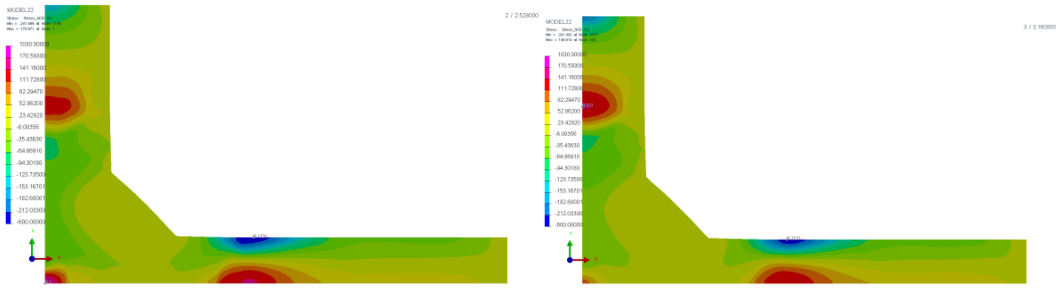

(1) (2)

Figure 4.32 residual stress σ_{xx} distribution during welding with the finer mesh for 316L (1) at= 2.52 (2) at t=3.16

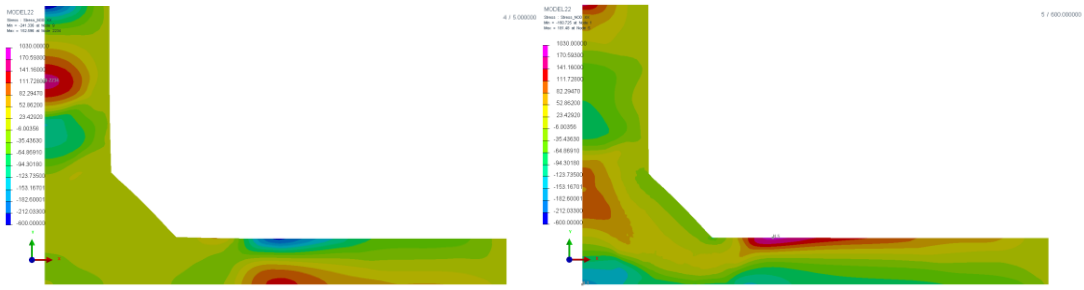

(1) (2)

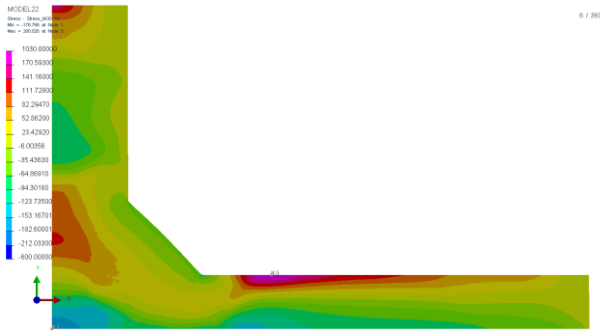

(3)

Figure 4.33 residual stress σ_{xx} distribution during cooling with the finer mesh for 316L (1) at t=5s (2) at t=600 s (3) at t=3600s

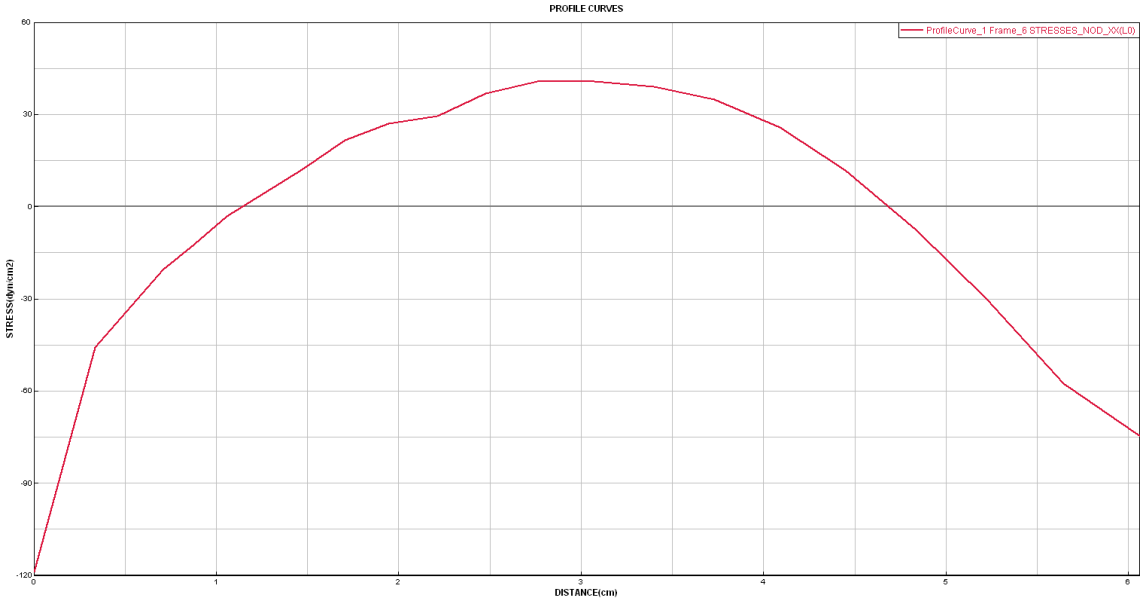

Figure 4.34 residual stress σ_{xx} measured from welded toe in y direction after cooling

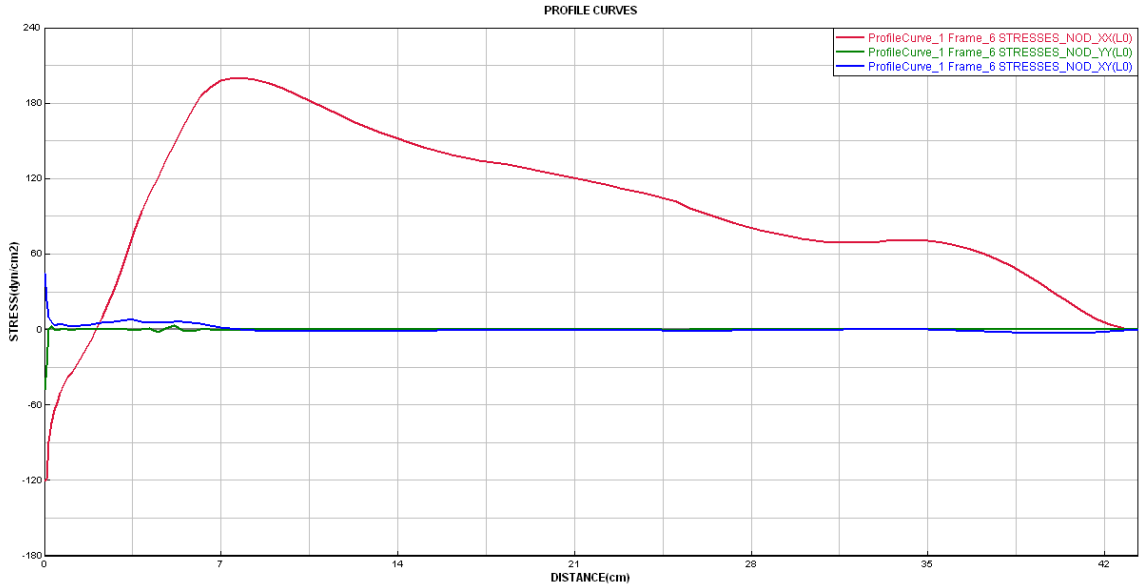

Figure 4.35 residual stresses σ_{xx}, σ_{xy}, σ_{yy} from the upper surface measured from welded toe in x direction

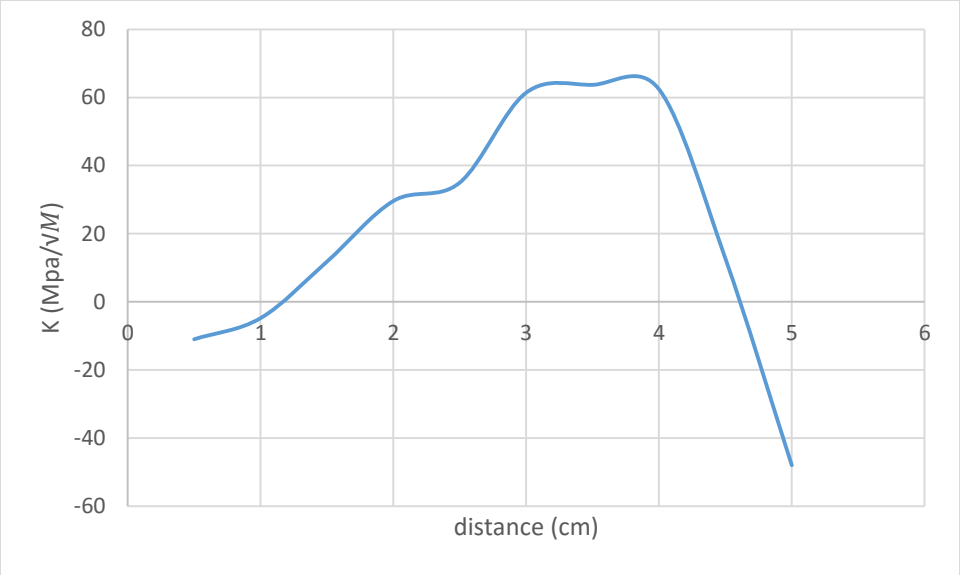

Figure 4.36 Stress intensity factors K (Mpa/$\sqrt{M}$) of different crack length measured from welded toe in Y direction

4.5 Conclusion

1. Comparing Figure 4.1, 4.2 in section 4.1, with Figure 4.10, 4.11 in section 4.2, temperature distribution has little difference. Thus material property has a little effect on temperature. Comparing Figure 4.1, 4.2 with Figure 4.19, 4.20, mesh quality affects little on temperature distribution.

2. Comparing Figure 4.3 with 4.4, or Figure 4.5 with 4.6 in section 4.1, the value of von Mises stresses and $\boldsymbol{\sigma_{xx}}$ residual stresses was little during welding, while grow rapidly during cooling process.

3. Comparing Figure 4.13 with Figure 4.31, the value of von Mises residual stresses has a difference between different meshes. Also, the Figure 4.4 shows that von Mises residual stresses are high in the vertical bar, while are low in the horizontal bar. I think the result of Figure 4.4 has some mistake for coarse mesh used in section 4.2

4. Comparing Figure 4.7 in section 4.1 with Figure 4.16 in section 4.2, we could find that austenitic stainless 316L steel have much higher stresses near the fillet weld toe than carbon S355J2G3 steel for the reason phase changing.

References

[1] Berge, S., and Eide, O. I., Residual Stress and Stress Interaction in Fatigue Testing of Welded Joints, in Residual Stress Effects in Fatigue, ASTM Technical Publication 776, ASTM 1916 Race Street, Philadelphia, PA, 19103, 1981, pp. 115-131.

[2] Baumgartner, J., and Bruder, T., Influence of Weld Geometry and Residual Stresses on the Fatigue Strength of Longitudinal Stiffeners, Weld World, Published Online: 12 July, 2013.

[3] Williams, M. L., Stress Singularities Resulting from Various Boundary Conditions in Angular Corners of Plates in Extension, Trans. ASME, J. of Applied Mech, Vol. 19, 1952, pp. 526-528.

[4] Bussu, G., Irving, P. E., The Role of Residual Stress and Heat Affected Zone Properties on Fatigue Crack Propagation in Friction Stir Welded 2024-T351 Aluminum Joints, International Journal of Fatigue, 2003.

[5] D. Stefanescu，L. Edwards，M.E. Fitzpatrick, Stress intensity factor correction for asymmetric through-thickness fatigue cracks at holes, International Journal of Fatigue, 25, 2003, pp. 569-576.

[6] S. Pommier, C. Sakae, Y. Murakami, An empirical stress intensity factor set of equations for a semi-elliptical crack in a semi-infinite body subjected to a polynomial stress distribution, International Journal of Fatigue, 21, 1999, pp. 243-251.

[7] Nguyen, T. Ninh and M. A., Wahab, The effect of residual stress and weld geometry on the improvement of fatigue life, Journal of Materials Processing Technology, 48, 1995, pp.581-588.

[8] R.J. Dexter, P.J. Pilarski, H. N. Mahmoud, Analysis of crack propagation in welded stiffened panels, International Journal of Fatigue, 25, 2003, pp. 1169-1174.

[9] Krishnakumar Shankar, Weidong Wu, Effect of welding and weld repair on crack propagation behaviour in aluminium alloy 5083 plates, Materials and Design, 23, 2002, pp. 201-208.

[10] HyperWorks Desktop User's Guide, 2012.

[11] SYSWELD 2010, Reference Manual, www.esi-group.com, Release January 2010.

[12] G. Labeas, S. Tsirkas, J. Diamantakos and A. Kermanidis, Effect of residual stresses due to laser welding on the Stress Intensity

[13] ANSYS®, User's manual, 2010.

[14] Mengel, A., Finite Element Modeling of LENS Deposition Using SYSWELD, M.S. Thesis, Lehigh University, 2002

[15] Nied, H., and Siegele, D., "Study of the Influence of Material and Welding Modeling on the Residual Stresses in Longitudinal Stiffeners," *66th Annual Assembly and International Conference, Commission XIII Fatigue of Welded Components and Structures,* Doc. XIII-2479-13, International Institute of Welding, Essen, Germany, Sept. 11-15, 2013.

[16] H. F. Nied, Welding Simulation Using SYSWELD: An Introductory Tutorial, IWM Bericht V999/2013

VITA

Changyuan Du was born on August 9, 1989 in Dalian, Liaoning Province in P.R. China. He has been at Lehigh University since 2013 as a graduate student in Department of Mechanical Engineering and Mechanics.